EFFECT OF LEAD FLUORIDE ON THE SPECTROSCOPIC PROPERTIES OF Dy^{3+}-DOPED BORATE-BASED GLASSES[**]

Priyanka Srivastava

K. N. Govt. P. G. College, Gyanpur, Bhadohi, India; e-mail: prriyaprakash@gmail.com

The effect of adding PbF_2 to the spectroscopic properties of dysprosium-doped borate-based glasses is studied. The content of PbF_2 in the glass is varied from 0 to 50 mol%. X-ray diffraction confirms the amorphous nature of the glass. The Judd–Ofelt theory is applied to evaluate the intensity parameters Ω_λ (λ = 1, 2, 3) from the UV-Vis-NIR absorption spectra of glasses. Various radiative parameters are calculated, and the variation of these parameters with different concentrations of lead fluoride is discussed. The fluorescence spectra of glasses are recorded, and it is observed that the fluorescence yield increases as the PbF_2 content rises from 0 to 40 mol% but decreases thereafter. The IR absorption spectra of these glasses are also recorded and interpreted in terms of changes in the structure of the glasses. The decay lifetime of the $^4F_{9/2}$ level of the dysprosium ion is measured from the decay profile and compared with the calculated lifetime.

Keywords: *borate glass, fluorescence, radiative properties, branching ratio, decay curve.*

ВЛИЯНИЕ ФТОРИДА СВИНЦА НА СПЕКТРОСКОПИЧЕСКИЕ СВОЙСТВА СТЕКОЛ НА ОСНОВЕ БОРАТА, ЛЕГИРОВАННОГО ИОНАМИ Dy^{3+}

P. Srivastava

УДК 535.372:549.691.1

Правительственный колледж, Гьянпур, Бхадохи, Индия;
e-mail: prriyaprakash@gmail.com

(Поступила 12 мая 2022)

Изучено влияние добавления PbF_2 на спектроскопические свойства некоторых стекол на боратной основе, легированных диспрозием. Содержание PbF_2 в стекле варьировалось от 0 до 50 мол.%. Аморфная природа стекла подтверждена с помощью рентгеновской дифракции. Параметры интенсивности Ω_λ (λ = 1, 2, 3) оценены по спектрам поглощения в УФ-видимой и ближней инфракрасной областях спектра с использованием теории Джадда–Офельта. Рассчитаны радиационные параметры и проанализировано их изменение при разных концентрациях фторида свинца. Зарегистрированы спектры флуоресценции стекол и обнаружено возрастание выхода флуоресценции по мере роста содержания PbF_2 от 0 до 40 мол.%, затем его снижение. Зарегистрированные ИК-спектры поглощения стекол интерпретированы с точки зрения изменения структуры стекол. Проведено сравнение времени жизни уровня $^4F_{9/2}$ иона диспрозия, измеренного по профилю распада, с рассчитанным временем жизни.

Ключевые слова: *боратное стекло, флуоресценция, радиационные параметры, коэффициент ветвления, кривая затухания.*

Introduction. Glasses doped with rare-earth ions have been used in a variety of technological applications such as photonics and optoelectronics as optical amplifiers [1, 2], laser materials [3, 4], display devices [5, 6], solid-state laser sensors [7–9], high-density optical memory devices [10], and amplifiers for fiber-optic communication [11, 12]. The optical properties of rare-earth ions strongly depend on the host glass ma-

[**]Full text is published in JAS V. 90, No. 1 (http://springer.com/journal/10812) and in electronic version of ZhPS V. 90, No. 1 (http://www.elibrary.ru/title_about.asp?id=7318; sales@elibrary.ru).

trix. For this reason, the host matrix is vital for the development of rare earth-doped optical devices [13]. Among different materials, phosphate borate glasses are one of the best and most well-known glass formers owing to their unique and attractive features such as ease of preparation, low melting point, high transparency, and chemical stability, good rare-earth ion solubility and, most importantly, low price [14, 15]. On the other hand, borate glasses have limitations owing to their high phonon energy, which enhances the nonradiative decay and reduces the quantum efficiency [16]. The borate glass network consists of a trigonal BO_3 unit in the form of boroxol rings connected by B-O-B linkage with the phonon energy 1300 cm^{-1}. When heavy metals are added to borate glasses as modifiers, the BO_3 units are converted into four coordinated BO_4; thus, reducing the phonon energy to 980 cm^{-1}. This in turn enhances the fluorescence yield of rare-earth ions, which leads to intense laser emission. Moreover, when a fluorine compound is added to any host, the phonon energy of the host decreases, and the OH content decreases too because fluorine reacts with OH and forms HF [17–19]. A large number of studies have been devoted to the preparation and characterization of the B_2O_3–PbO/PbF_2 system [20–24].

Among different rare-earth ions, Dy^{3+} ions are considered to be the best because of two most intense bands in the visible spectral region that correspond to $^4F_{9/2}$–$^6H_{15/2}$ (blue) and $^4F_{9/2}$–$^6H_{13/2}$ (yellow) transitions [25–27]. The spectroscopic and luminescent properties of Dy^{3+} ions have been investigated in various hosts. The luminescence properties of Dy^{3+} ions in boro tellurite glass were studied by K. Reddy et al., who proposed that this host is promising for optoelectronic applications [28]. The spectroscopic properties of Dy^{3+}-doped oxyfluoride glasses for white emitting diodes were reported by K. V. Krishnaih et al. [29]. The luminescence properties of the dysprosium ion were studied by Suthanthirakuma and Marimuthu [30] and Venkata Rao et al. [31]; they reported that it is a suitable ion for the development of new laser materials.

Experimental. Dy^{3+}-doped borate glasses with different concentrations of lead fluoride were prepared using the melt quenching technique with the following chemical composition:

$$68H_3BO_3 + 20Li_2CO_3 + (10 - x)\,CaCO_3 + xPbF_2 + 2Dy_2O_3,\ x = 0, 1, 3, 10;$$
$$68H_3BO_3 + (20 - y)\,Li_2CO_3 + (10 + y)\,PbF_2 + 2Dy_2O_3,\ y = 10, 20;$$
$$(68 - z)\,H_3BO_3 + (30 + z)\,PbF_2 + 2Dy_2O_3,\ z = 10, 20.$$

The numbers appearing before the chemical symbols denote the concentration in mol%. These compounds were thoroughly crushed in an agate mortar to mix them homogeneously. Next the mixture was placed in a platinum crucible and melted in an electric furnace at 1100°C for 1 h. Then the melt was air quenched by pouring it on a rectangular iron cast kept at 500°C. It was then slowly cooled to room temperature to get a properly annealed glass and then polished to achieve good transparency. The refractive indices of these glasses were measured by Brewster's angle method using a He–Ne laser as a source (650 nm). We tested the glasses formed in this manner to ensure their noncrystalline character through X-ray diffraction. The XRD of the prepared glasses was recorded by an X-ray diffractometer (Philips PW1710). The UV-Vis-NIR absorption spectra of the glasses were recorded using a Cary-2390 VARIAN double-beam spectrophotometer. In all the absorption measurements, the glass host (without rare earth) was used for the reference beam transmission. The fluorescence spectra of the glasses were recorded using a 476.5-nm line of a Coherent 10-watt Ar^+ Laser with 400 MW power and a bandwidth of 0.01 nm. The fluorescence signal was dispersed by a Spex 0.5 m monochromator and detected by an IP21 PMT.

Results and discussion. To check the amorphous nature of the prepared glasses, the XRD spectral measurements were taken for all of the glasses and the XRD spectrum showed a broad hump, which was characteristic of an amorphous material. This confirms the amorphous nature of the prepared glasses.

The infrared spectra of the Dy^{3+}-doped glasses with and without lead fluoride are shown in Fig. 1. The vibrational modes of the borate network are seen mainly in three energy regions 1600–1200, 1200–800, and 700–450 cm^{-1}), which are similar to those reported by other researchers [32, 33]. The first group of bands, which is in the 1200–1600 cm^{-1} region, is due to the asymmetric stretching vibration of the B-O bond of the trigonal units. The second group lies between 800 and 1200 cm^{-1}, and it is due to the B-O bond stretching of the tetrahedral BO_4 units. The third group is observed between 450 and 700 cm^{-1}, and it is due to the bending of the B-O-B linkage in the borate networks. It can be seen from Fig. 2 that the peaks corresponding to the first and second groups become broader and weaker with the addition of lead fluoride. An increase in PbF_2 has little effect on the third group of peaks. The peak at 1266 cm^{-1} is observed only in PbF_2-free glass, and this peak is due to the boroxol ring. The disappearance of this peak means that boroxol rings are broken in the presence of PbF_2. A similar disappearance of this vibrational peak is observed with the addition of PbO but for a high PbO concentration (50–60%) the peak reappears [32]. The peak observed at 1401 cm^{-1}

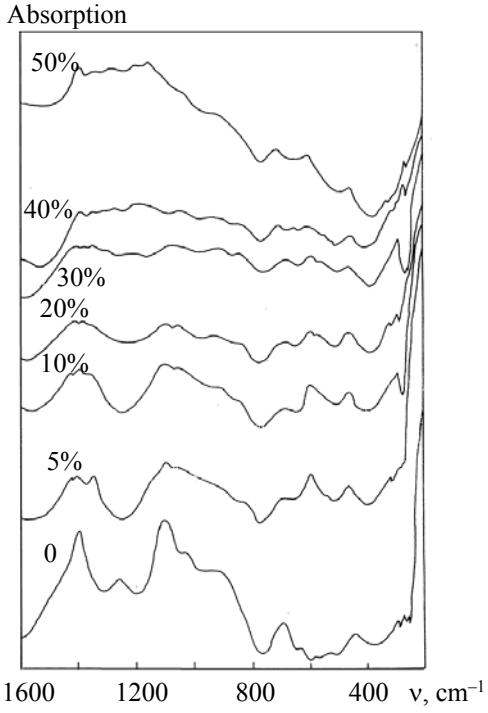

Fig. 1. Infrared absorption spectra of Dy^{3+}-doped borate-based glasses at different concentrations of lead fluoride.

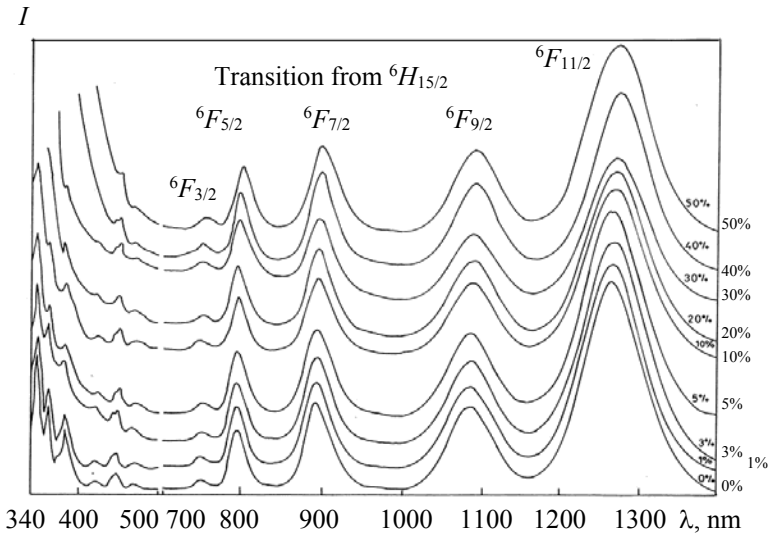

Fig. 2. UV-Vis-NIR absorption spectra of Dy^{3+}-doped borate-based glasses at different concentrations of lead fluoride.

in the absence of PbF_2 is shifted toward lower wave numbers with the addition of PbF_2. This peak becomes broader and weaker with increasing concentration of PbF_2, but the intensity increases again when the concentration of PbF_2 is >50 mol%. At the 5% concentration of PbF_2 there is an absorption peak at 1334 cm^{-1}, which is assigned to the vibration of the (BIII-O-B IV) group [34]. It appears only as a shoulder of a strong peak seen at 1382 cm^{-1} at higher concentrations of lead fluoride. In the region 800–1200 cm^{-1}, one can see an intense peak at 1110 cm^{-1} and peaks at 1036 and 916 cm^{-1} when no PbF_2 is present. The peak at 1110 cm^{-1}attributed to the B-O vibration of the BO_4 unit is shifted toward the lower frequencies (seen at 1083 cm^{-1} for glass with the PbF_2 concentration ~20%). The peak observed at 1036 cm^{-1} is due to the diborate group and the one at 916 cm^{-1} is due to the orthoborate group. When the concentration of lead fluoride is low, the bands due to BO_3 and BO_4 stretching are well separated but with increasing concentration

of PbF_2 these bands become broader and overlap, so they cannot be separated. The intensity of the peaks due to the BO_3 group decreases for the addition of lead fluoride and at 20 mol% of PbF_2 becomes equal to the intensity of the bands because of the BO_4 group. This indicates that BO_4 groups increase at the expense of BO_3. For a higher concentration of PbF_2 one can see a partial recovery in the intensity of BO_3 bands. For the PbF_2 concentration of 50%, the peak at 1036 cm^{-1} has a lower intensity, but the peak at 890 cm^{-1} remains virtually unaffected. This indicates that a back conversion of BO_4 into BO_3 with three coordinated boron atoms in the form of an orthoborate group takes place.

The absorption spectra of these glasses for all concentrations of lead fluoride are shown in Fig. 2. Each spectrum consists of six main absorption peaks corresponding to the transition from the ground state $^6H_{15/2}$ to various excited states $^4I_{11/2}$, $^6F_{3/2}$, $^6F_{5/2}$, $^6F_{7/2}$, $^6F_{9/2}$, and $^6F_{11/2}$ of the dysprosium ion [35]. The peak positions and corresponding transitions are given in Table A1. The absorption peaks in the region 340–500 nm are very weak owing to the strong absorption of the glass host in this region. The absorption edge in this region shifts toward the higher wavelength side with increasing concentration of PbF_2. This is in agreement with earlier works in that the increasing concentration of metal oxides such as Na_2O, K_2O, and PbO, etc., shifts the absorption edge to longer wavelengths [36, 37]. The intensity and the width of the absorption bands in the region 700–1500 nm vary very little with an increase in the lead fluoride content. The position and intensity of certain electric dipole transitions in rare-earth ions are found to be very sensitive to the environment of the ion. Such transitions are termed hypersensitive transitions. Jorgensen and Judd [38] noted that all known hypersensitive transitions obey the selection rules $|\Delta S| = 0$, $|\Delta L| \le 2$, $|\Delta J| \le 2$. For the Dy^{3+} ion, the transition, $^6H_{15/2} \rightarrow {}^6F_{11/2}$, is a hypersensitive transition. The spectral intensity for this transition is large compared with other transitions of Dy^{3+} and the peak wavelength of this transition shifts toward the higher wavelengths with increasing concentration of lead fluoride. In order to find out the nature of bonding in the present glasses, the nephelauxetic ratio $\beta = \nu_c/\nu_a$ and the bonding parameter $\delta = [(1 - \bar{\beta})/\bar{\beta}]\times 100$ [39] are used, where ν_c is the wave number of the particular Dy^{3+} transitions in the present host, ν_a is the wave number of the same transition in an aqua ion [37, 40], and $\bar{\beta}$ is the average value of β. Depending upon the surrounding environment around the rare-earth ions, the bonding parameter δ may be positive or negative indicating covalent or ionic bonding respectively. The values of $\bar{\beta}$ and δ for all glasses are calculated and presented in Table 1. The values of the bonding parameter δ are negative indicating that the bonding between the Dy^{3+} and the surrounding ligands in the glass matrix is ionic. This ionic nature of bonding continues to decrease with the lead fluoride content in these glasses. The spectral intensities of absorption bands are expressed by the experimental oscillator strength (f_{exp}) and are obtained by using the area under the absorption curve employing the expression given in Zhang et al. [41]. The Judd–Ofelt theory [42–44] was applied to the experimentally observed oscillator strengths to obtain the Judd–Ofelt intensity parameters (Ω_2, Ω_4, Ω_6) and the calculated oscillator strength (f_{cal}) by the least square fit method. The root mean square deviations are also calculated, and smaller values indicate the good fit between the experimental and calculated oscillator strength and the validity of the Judd–Ofelt theory. The experimental (f_{exp}) and calculated (f_{cal}) values of the oscillator strength, together with the root mean square deviations and refractive indices of glasses, are given in Table 1.

The calculated values of the Judd–Ofelt intensity parameters for all glass matrices, their trends, along with the values reported by others, are given in Table 2. A comparison of the Judd–Ofelt intensity parameters in various glass systems are also given in Table 2.

The Judd–Ofelt intensity parameters of the Dy^{3+}-doped borate-based glass matrix for all concentrations of lead fluoride are found to be similar and comparable with the values reported by other glass matrices. The tendency of the Judd–Ofelt parameters is $\Omega_2 > \Omega_6 > \Omega_4$ for the present glass matrices. The intensity parameter Ω_2 depends on the covalent nature between Dy^{3+} ions and the ligand anion and is directly associated with the asymmetry of the local environment around rare-earth ions where the intensity parameters Ω_4 and Ω_6 are related to the bulk properties such as the rigidity and viscosity of the medium in which the rare-earth ions are situated [44]. When the Judd–Ofelt parameters for the present glass system are compared with the other reported values given in Table 3, it can be seen that the value of the intensity parameter Ω_2 is smaller, indicating a higher degree of symmetry around the Dy^{3+} ion and a strong ionic bond (weaker covalency) between Dy and O. It is also confirmed by the nephelauxetic ratio (β) and the bonding parameter (δ). However, the intensity parameter Ω_2 decreases with the addition of lead fluoride, having a 30% minimum value of PbF_2. It increases again for 40% of PbF_2 and then decreases. Ω_4 and Ω_6 do not show any appreciable change after an initial decrease. The minimum value of Ω_2 at 30 mol% of lead fluoride indicates the higher degree of symmetry of the ligand field around the rare-earth and the weaker covalency of the Dy–O bond. From the IR

spectra, it is observed that the addition of PbF_2 to borate-based glass converts BO_3 to BO_4, resulting in the conversion of the boroxol group to pentaborate and diborate groups, and this fraction of BO_4 is maximal near about 20–30% of PbF_2. This excess formation of BO_4 leads to the close packing of oxygen atoms around the rare-earth ion [45] and so decreases the asymmetry of the crystal field at the rare-earth site. With the further addition of lead fluoride, the back conversion of BO_4 to BO_3 with the formation of nonbridging oxygen takes place, which leads to an increase in the distortion of the ligand field at the rare-earth site; thus, the value of Ω_2 increases. The variation of the intensity parameter Ω_2 is also consistent with the nature of the bonding pa rameter δ. The intensity parameter Ω_6 is associated with the rigidity of the host material, and it is expected that its value will be increasing owing to the tightening of the structure with the formation of BO_4, but its value continues to decrease with the lead fluoride content. The spectroscopic quality factor (χ), which is the ratio of Ω_4 and Ω_6, characterizes the lasing property of the material [47]. It is calculated and given in Table 3. In the present series, its value is maximal for the glass matrix with 30% PbF_2.

TABLE 1. Experimental Oscillator Strength ($f_{exp}\times10^{-8}$), Calculated Oscillator Strength ($f_{exp}\times10^{-8}$), the Root Mean Square Deviation (δ_{rms}), Bonding Parameters $\bar{\beta}$, δ, and Refractive Index (n) of Dy^{3+}-Doped Glasses with Different Concentrations of PbF_2

From ground state	Oscillator strength×10^{-8}								
	E, cm^{-1}	f_{exp}	f_{cal}	E, cm^{-1}	f_{exp}	f_{cal}	E, cm^{-1}	f_{exp}	f_{cal}
$^6H_{15/2}$	0% PbF_2			10% PbF_2			20% PbF_2		
$^6F_{11/2}$	7924	291	291	7862	254	254	7862	214	214
$^6F_{9/2}$	9260	145	141	9208	119	117	9191	125	137
$^6F_{7/2}$	11,186	119	140	11,161	104	113	11161	126	138
$^6F_{5/2}$	12,531	80	71	12,531	53	57	12563	66	70
$^6F_{3/2}$	13,405	12	13	13,333	7	10	13369	12	13
$^4I_{15/2}$	22,272	32	29	22,124	22	28	22222	25	29
δ_{rms}	±0.043			±0.034			±0.056		
$\bar{\beta}$	1.014			1.010			1.010		
δ	−1.38			−0.99			−0.99		
n	1.50			1.83			1.87		
	30% PbF_2			40% PbF_2			50% PbF_2		
$^6F_{11/2}$	7849	235	235	7843	251	251	7825	228	228
$^6F_{9/2}$	9174	107	104	9157	124	122	9157	118	117
$^6F_{7/2}$	11,161	77.0	92.0	11,136	114	121	11,111	113	118
$^6F_{5/2}$	12,531	53.0	44.0	12,531	54.0	61.0	12,500	51.0	60.0
$^6F_{3/2}$	13,333	11.0	8.00	13,333	13.0	11.0	13,298	11.0	11.0
$^4I_{15/2}$	22,124	17.0	18.0	22,124	11.0	21.0	22,222		
δ_{rms}	±0.057			±0.057			±0.037		
$\bar{\beta}$	1.009			1.008			1.008		
δ	−0.89			−0.79			−0.79		
n	1.96			2.01			2.07		

TABLE 2. Judd–Ofelt Intensity Parameters [(Ω_2, Ω_4, Ω_6)×10^{-20}] and Spectroscopic Quality Factor χ for Dy^{3+} Ions in Borate-based Glasses with Different Concentrations of Lead Fluoride

Glass system	Ω_2	Ω_4	Ω_6	χ	Trend	References
0% PbF_2	3.608	0.716	1.954	0.366	$\Omega_2 > \Omega_6 > \Omega_4$	Present work
10% PbF_2	2.270	0.483	1.127	0.428	$\Omega_2 > \Omega_6 > \Omega_4$	Present work
20% PbF_2	1.790	0.516	1.107	0.466	$\Omega_2 > \Omega_6 > \Omega_4$	Present work
30% PbF_2	1.660	0.597	0.768	0.770	$\Omega_2 > \Omega_6 > \Omega_4$	Present work
40% PbF_2	1.930	0.404	1.040	0.388	$\Omega_2 > \Omega_6 > \Omega_4$	Present work
50% PbF_2	1.660	0.318	0.976	0.320	$\Omega_2 > \Omega_6 > \Omega_4$	Present work

Continue Table 2

Glass system	Ω_2	Ω_4	Ω_6	χ	Trend	References
PTBDY10	7.75	2.31	2.70	0.855	$\Omega_2 > \Omega_6 > \Omega_4$	[32]
Lead borate	4.90	0.94	2.07	0.45	$\Omega_2 > \Omega_6 > \Omega_4$	[44]
LCZSFBDy 10	11.25	2.45	5.16		$\Omega_2 > \Omega_6 > \Omega_4$	[45]
PbF_2-WO_3-TeO_2	5.19	1.93	1.07	1.80	$\Omega_2 > \Omega_6 > \Omega_4$	[18]
Dy:LiLTB	8.65	2.62	2.07	1.26	$\Omega_2 > \Omega_6 > \Omega_4$	[46]

TABLE 3. Radiative Transition Probabilities (A_R) (s^{-1}), Total Radiative Transition Probability (A_T) (s^{-1}), Branching Ratios (β_R), and Radiative Lifetime (τ_R) (ms) of Dy^+-Doped Borate-based Glasses for Various Concentrations of Lead Fluoride

Transition from $^4F_{9/2}$	Parameter	0% PbF_2	10% PbF_2	20% PbF_2	30% PbF_2	40% PbF_2	50% PbF_2
$^6H_{11/2}$	A_R	32.00	40.11	33.75	40.39	48.34	46.90
	β_R	0.06	0.06	0.05	0.06	0.06	0.06
$^6H_{13/2}$	A_R	351.76	433.68	389.33	427.52	531.09	524.31
	β_R	0.68	0.67	0.65	0.67	0.69	0.54
$^6H_{15/2}$	A_R	123.29	144.62	154.18	132.54	185.79	192.5
	β_R	0.23	0.22	0.25	0.21	0.33	0.23
A_T		523.79	641.12	596.96	623.14	790.72	780.50
τ_R		1.91	1.56	1.67	1.60	1.26	1.28

Radiative properties and fluorescence spectra. The fluorescence spectra of Dy^{3+} ion-doped glasses with varying concentrations of lead fluoride is recorded on excitation with a 476.5-nm line of an Ar^+ laser at room temperature, as shown in Fig. 3. The energy corresponding to the 476.5-nm line of the laser is 20,986 cm^{-1}, and it is very close to the excitation energy of $^4F_{9/2}$ (20,986 cm^{-1}). Therefore, this level gets populated, and the fluorescence is observed from this level. In the fluorescence spectrum, only two peaks at 577 and 669 nm are observed corresponding to the transitions $^4F_{9/2}\rightarrow{}^6H_{13/2}$ (yellow) and $^4F_{9/2}\rightarrow{}^6H_{11/2}$ (red), respectively. A peak at 482 nm seen by other workers is not observed in our experiment, probably because of its closeness with the exciting line. Among these two transitions, the transition $^4F_{9/2}\rightarrow{}^6H_{13/2}$ in the yellow region is a hypersensitive transition obeying the selection rules. It can be seen from the fluorescence spectra that the intensity of the fluorescence transitions increases with increasing concentration of PbF_2, reaching a maximum at 40% of PbF_2 and then decreasing. At 40% of PbF_2 the intensity of the peak at 577 nm is almost 6 times the intensity observed in the absence of PbF_2. The enhancement in fluorescence is probably attributed to the structural change in the glasses due to lead fluoride. With the addition of PbF_2 there is conversion of BO_3 to BO_4 in the glass, which reaches a maximum when the PbF_2 concentration is within the range 30–40%, which leads to a reduction in the phonon energy in the glass matrix. This may be the reason for the enhanced fluorescence as the reduced phonon frequency decreases the rate of nonradiative relaxation.

The Judd–Ofelt parameters (Ω_λ) obtained from the absorption measurements and refractive index can be used to describe the radiative properties of the fluorescing levels for rare-earth ions in the glass host. The radiative properties such as transition probability (A_R), total transition probability, branching ratios (β_R) radiative lifetime (τ_R) of the excited level $^4F_{9/2}$ of Dy^{3+} were calculated using the expressions given in SouzaFilho et al. [48] and listed in Table 3.

The radiative branching ratio β_R is a parameter that decides the capability of acquiring stimulated emission from any particular transition if its value of $\beta_R \geq 0.50$. In the present work the value of β_R is larger for the emission transition $^4F_{9/2}\rightarrow{}^6H_{13/2}$ (see Table 4). The effective bandwidths ($\Delta\lambda_{eff}$, nm), stimulated emission cross section ($\sigma_e\times10^{-22}$ cm^2), and gain bandwidth parameter [$(\sigma_e\times\Delta\lambda_{eff})\times10^{-28}$ cm^3] for $^4F_{9/2}\rightarrow{}^6H_{13/2}$ transition of 2.0 mol% of Dy^{3+}-doped borate-based glass for different concentrations of lead fluoride indicate that this transition has more potential for laser emission. On the other hand, the values of the radiative transition probability and branching ratio have the largest value for the glass containing 40% lead fluoride, indicating that this glass system can be used as an effective laser system in the yellow region. The other radiative properties, such as effective bandwidths ($\Delta\lambda_{eff}$), stimulated emission cross section (σ_e), and gain bandwidth parameter ($\sigma_e\,\Delta\lambda_{eff}$) for $^4F_{9/2}\rightarrow{}^6H_{13/2}$ transition are calculated from fluorescence spectra and tabulated in Table 4.

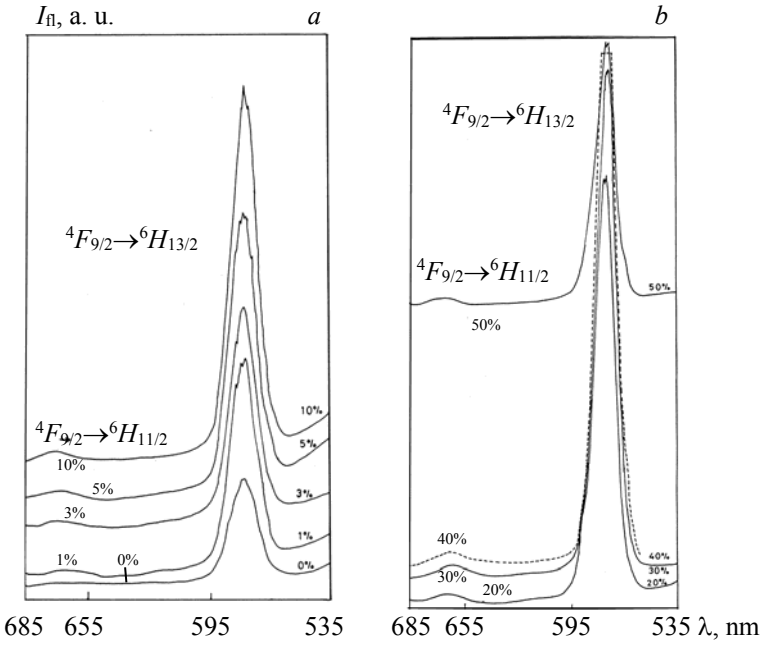

Fig. 3. Fluorescence spectra of Dy^{3+}-doped borate-based glasses at different concentrations of lead fluoride.

TABLE 4. Effective Bandwidths ($\Delta\lambda_{eff}$, nm), Stimulated Emission Cross Section ($\sigma_e\times10^{-22}$ cm^2) and Gain Bandwidth Parameter [$(\sigma_e\times\Delta\lambda_{eff})\times10^{-28}$ cm^3] for $^4F_{9/2}\rightarrow{}^6H_{13/2}$ Transitions of 2.0 mol% of Dy^{3+}-doped Borate-based Glass for Different Concentrations of Lead Fluoride

Concentrations of PbF_2, %	$\Delta\lambda_{eff}$, nm	$\sigma_e\times10^{-22}$ cm^2	$(\sigma_e\times\Delta\lambda_{eff})\times10^{-28}$ cm^3
0	15.5	14.2	22.01
10	14.5	12.2	17.69
20	14.5	11.3	16.85
30	13.3	11.7	15.56
40	12.1	15.1	18.27
50	13.1	14.1	18.47

The laser performance of a material is characterized by radiative parameters, i.e., stimulated emission cross section. From Table 4, it can be seen that its value is the highest for the glass containing 40% lead fluoride. Also, the effective bandwidth is the smallest for this composition of glass, which suggests that the transition $^4F_{9/2}\rightarrow{}^6H_{13/2}$ is the sharpest for this glass system. The highest value of transition probability (A_R), branching ratio (β_R), stimulated emission cross section (σ_e), and the smallest value of effective band width ($\Delta\lambda_{eff}$) for glass containing 40% of lead fluoride prove that this glass is the most suitable host for low-threshold, high-gain laser emission at 577 nm. Rare-earth-doped glasses can act as better optical fiber if the gain width parameter ($\sigma_e\times\Delta\lambda_{eff}$) has a higher value [49]. The higher value of the gain width parameter for these glass systems indicates that these are used in optical amplification.

Fluorescence decay analysis. The fluorescence decay curves originating from the excited level $^4F_{9/2}$ of Dy^{3+} ions in these glasses were recorded and shown in Fig. 4. We measured the lifetime of the fluorescing level $^4F_{9/2}$ of Dy^{3+} ions in glasses containing 0, 40, and 50% lead fluoride. The logarithmic decay curves are shown in Fig. 4 and the experimentally measured lifetimes (τ_{exp}) are 1.162, 0.937, and 0.945 ms, respectively, for glasses with 0, 40, and 50% of PbF_2. The measured lifetimes (τ_{exp}) for the present glass systems are found to be larger than other Dy^{3+} ions-doped glasses [28, 49–52]. It is seen that the lifetime(τ_{exp}) is the smallest for 40% of lead fluoride. The value of the measured lifetime (τ_{exp}) is also smaller than the calculated value of the radiative life time (τ_R). This is probably due to the presence of nonradiative decay processes.

The total decay rate (τ_{exp}) of a fluorescent level is the sum of the radiative ($A_T = \tau_R$) and nonradiative decay rates (W_{NR}) [53]: $1/\tau_{exp} = A_T + W_{NR}$. Hence, the nonradiative relaxation rate $W_{NR} = (1/\tau_{exp}) + (1/\tau_R)$. The nonradiative relaxation rates of the $^4F_{9/2}$ level of Dy^{3+} ions in the present glasses were calculated for 0, 40, and 50 of PbF_2 and are found to be 336.8, 276.5, and 277.7 s^{-1}, respectively. It is noted that the nonradiative relaxation rate decreases with the addition of lead fluoride in borate-based glasses, which in turn supports the enhancement in the fluorescence intensity with increasing concentration of lead fluoride. The quantum efficiency may be defined as the ratio of a measured life time ($1/\tau_{exp}$) and radiative life time ($1/\tau_R$): $\eta = (\tau_{exp}/\tau_R)\times 100$.

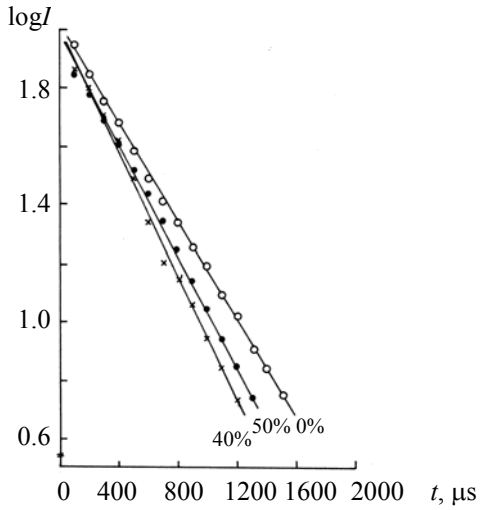

Fig. 4. Log*I* versus time curve for $^4F_{9/2}\rightarrow{}^6H_{13/2}$ transition for different concentrations of PbF_2 in borate-based glasses: 0 (○), 40 (×), and 50% (•)

TABLE 5. Experimental Lifetime (τ_{exp}), Radiative Lifetime (τ_R), Quantum Efficiency (η%) and Nonradiative Relaxation Rate (W_{NR}) (s^{-1}) for Dy^{-3+}-Doped Borate-based Glasses for Different Concentrations of Lead Fluoride

% PbF_2	τ_{exp}, ms	τ_R, ms	η, %	W_{NR}, s^{-1}
0	1.162	1.91	60	336.79
40	0.937	1.26	74	276.51
50	0.945	1.28	73	277.70

The experimental life time (τ_{exp}), radiative life time (τ_R), quantum efficiency (η%), and nonradiative relaxation rate (W_{NR}, s^{-1}) for the present work are given in Table 5. It is clear that the glass containing 40% of PbF_2 with a low nonradiative relaxation rate and high quantum efficiency is the most suitable for optoelectronic applications.

Conclusions. The Dy^{3+}-doped borate-based glasses with different concentrations of lead fluoride were prepared using the melt quenching technique. These glasses were characterized through XRD, IR absorption, UV-Vis-NIR absorption, fluorescence, and decay rate measurements. The absorption spectra of all glasses were analyzed by using the Judd–Ofelt theory. The intensity parameters and their variation with the PbF_2 content correlate with the structural changes in the glass, as evidenced by the IR spectrum. The smaller the value of the Judd–Ofelt intensity parameter Ω_2, the higher the degree of symmetry around the Dy^{3+} ion and the stronger the ionic bond (weaker covalency) between Dy-O. It is observed from the fluorescence spectra that the intensity of transition $^4F_{9/2}\rightarrow{}^6H_{13/2}$ in the yellow region of the Dy^{3+} ion increases with increasing concentration of lead fluoride and is maximal for 40% of lead fluoride. With the help of the Judd–Ofelt intensity parameters and fluorescence spectra various radiative parameters such as transition probability, branching ratio, stimulated emission cross section, and quantum efficiency were calculated for all glasses. Among all glasses, glass containing 40% of PbF_2 has better radiative properties. Hence, it can be concluded that Dy^{3+}-doped borate-based glass with 40% lead fluoride is a promising optoelectronic device for yellow laser applications.

REFERENCES

1. M. P. Belancon, J. D. Marconi, M. F. Ando, L. Barbosa, *Opt. Mater*., **36**, 1020–1026 (2014).
2. A. Langar, C. Bouzidi, H. Elhouichel, M. Ferid, *J. Lumin*., **148**, 249–255 (2014).
3. J. Pisarska, L. Zur, W. A. Pisarski, *Spectrochim. Acta A*, **79**, 705–707 (2011).
4. P. Srivastava, S. B. Rai, D. K. Rai, *J. Alloys Compd*., **368**, 1–4 (2004).
5. G. Poirier, F. S. Ottoboni, F. C. Cassanjes, A. Remonte, Y. Messaddeq, S. J. L. Ribeiro, *J. Phys. Chem. B*, **112**, 4481–4487 (2008).
6. M. Ohtsuki, R. Tamura, S. Takeuchi, S. Yoda, T. Ohmura, *Appl. Phys. Lett*., **84**, 4911–4913 (2004).
7. L. Zhang, G. Dong, M. Peng, J. Qiu, *Spectrochim. Acta A*, **93**, 223–227 (2012).
8. I. Pal, A. Agarwal, S. Sanghi, M. P. Aggarwal, *J. Alloys Compd*., **509**, 7625–7631 (2011).
9. M. Olivier, P. Pirasteh, J. L. Doualan, P. Camy, H. Lhermite, J. L. Adam, V. Nazabal, *Opt. Mater*., **33**, 980–984 (2011).
10. C. W. Thiel, T. Bottger, R. L. Cone, *J. Lumin*., **131**, 353–361 (2011).
11. V. Nazabal, M. Poulain, M. Olivier, P. Pirasteh, P. Camy, J. L. Doualan, S. Guy, T. Djouama, A. Boutarfaia, J. L. Adam, *J. Fluor. Chem*., **134**, 18–23 (2012).
12. V. Krasteva, D. Machewirth, G. H. Sigel Jr., *J. Non-Cryst. Solids*, **213**, 304–310 (1997).
13. K. Nanda, R. S. Kundu, I. Pal, R. Punia , N. Kishore, *J. Alloys Compd*., **676**, 521–526 (2016).
14. I. I. Kindrat, B. V. Padlyak, R. Lisiecki, *Opt. Mater*., **49**, 241–248 (2015).
15. K. Linganna, Ch. Basavapoornima, C. K. Jayashankar, *Opt. Commun*., **344**, 100–105 (2015).
16. S. S. Sundari, K. Marimuthu, S. Shivraman, S. S. Babu, *J. Lumin*., **130**, 1313–1319 (2010).
17. Sk. Mahamuda, K. Swapna, M. Venkateswarlu, A. Srinivasa Rao, S. L. Shakya, G. Vijaya Prakash, *J. Lumin*., **154**, 410–424 (2014).
18. A. Mohan Babu, B. C. Jamalaiah, J. Suresh Kumar, T. Sasikala, L. Rama Moorthy, *J. Alloys Compd.*, **509**, 457–462 (2011).
19. D. Umamaheswari, B. C. Jamalaiah, T. Chengaih, G. Kim, L. Rama Moorthy, *Phys. Chem. Glasses*, **53**, No. 6, 271–275 (2012).
20. B. Klimesz, G. Dominiak-Dzik, R. Lisiecki, W. Ryba-Romanowski, *J. Non-Cryst. Solids*, **354**, 515−520 (2008).
21. G. Anjaiah, S. N. Rasool, P. Kistaiah, *J. Lumin*., **159**, 110−118 (2015).
22. R. G. Fernandes, J. Ren, A. S. S. de Camargo, A. C. Hernandes, H. Eckert, *J. Phys. Chem. C*, **116**, 6434–644 (2012).
23. W. A. Pisarski, T. Goryczka, J. Pisarska, W. Ryba-Romanowski, *J. Phys. Chem*., **111**, 2427−2430 (2007).
24. C. Doerenkamp, E. Carvajal, C. J. Magon, W. J. G. J. Faria, J. Pedro Donoso, Y. Galvao Gobato, A. S. S. de Camargo, H. Eckert, *J. Phys. Chem. C*, **123**, 22478−22490 (2009).
25. K. Kidsiri, J. Kaewkhao, H. J. Kim, Paper Presented at International Conference on Industrial Application Engineering, Institute of Industrial Applications Engineers, Japan (2016).
26. S. Babu, V. R. Prasad, D. Rajesh, Y. C. Ratnakaram, *J. Mol. Struct*., **1080**, 153–161(2015).
27. V. P. Tuyen, *J. Sci. Math. Phys*., **32**, No. 2 (2016).
28. K. Siva Rama Krishna Reddy, K. Swapna, S. K. Mahamuda, M. Venkateswarlu, A. S. Rao, G. Vijaya Prakash, *Opt. Mater*., **85**, 200–210 (2018).
29. K. V. Krishnaih, K. U. Kumar, C. K. Jayashankar, *Mater. Express*, **3**, 61–70 (2013).
30. P. Suthanthirakuma, K. Marimuthu, *J. Mol. Struct*., **1125**, 443–452 (2016).
31. K. Venkata Rao, Y. C. Ratnakaram, S. Babu, G. Venkataiah, Y. C. Ratnakaram, *J. Mol. Struct*., **1094**, 274–280 (2015).
32. P. Srivastava, S. B. Rai, D. K. Rai, *Spectrochim. Acta A*, **59**, 3303–3311 (2003).
33. C. R. Gautam, A. R. Yadav, *ISRN Ceram.*, 2–18 (**2012**).
34. A. A. Ahmed, N. A. Elshafi, M. R. Eltohamy, *Ind. J. Pure Appl. Phys*., **36**, 335 (1998).
35. M. V. Vijaya Kumar, B. C. Jamalaiah, K. RamaGopal, R. R. Reddy, *J. Lumin*., **132**, 86–90 (2012)
36. C. Dayanand, R. V. G. K. Sharma, G. Bhikshamaiah, M. Salagram, *J. Non-Cryst. Sol*., **167**, 122–128 (1994).
37. R. Nadjd-Sheibani, C. A. Hogarth, *J. Mat. Sci*., **26**, 429 (1991).
38. C. K. Jorgensen, B. R. Judd, *Mol. Phys*., **8**, 281 (1964).
39. D. D. Ramteke, A. Balakrishna, V. Kumar, H. C. Swart, *Opt. Mater*., **64**, 171–178 (2017).

40. W. T. Carnall, P. R. Fields, K. Rajnak, *J. Chem. Phys*., **49**, 4424 (1968).
41. F. Zhang, Z. F. Bi, A. Huang, Z. Xia, *J. Lumin*., **160**, 85–89 (2015).
42. B. R. Judd, *Phys. Rev.*, **127**, 750–761 (1962).
43. G. S. Ofelt, *J. Chem. Phys.*, **37**, 511–520 (1962).
44. J. Pisarska, *J. Phys.: Condens. Matter*, **21**, 285101 (2009).
45. C. Madhukar Reddy, B. Deva Prasad Raju, N. John Sushma, N. S. Dhoble, S. J. Dhoble, *Renewable and Sustainable Energy Rev*., **51**, 566–584 (2015).
46. S. A. Saleem, B. C. Jamalaiah, M. Jayasimhadri, K. Jang, L. Rama Moorthy, *J. Quant*. *Spectrosc. Radiat. Transfer*, **112**, 78 (2011).
47. C. K. Jorgensen, R. Reisfeld, *J. Less-Common Met*., **93**, 107–112 (1983).
48. A. G. SouzaFilho, J. MendesFilho, F. E. A. Melo, M. C. C. Custodio, R. Lebullenger, A. C. Hernandes, *J. Phys. Chem. Solid*, **61**, 1535 (2000).
49. K. Swapna, Sk. Mahamuda, A. Srinivasa Rao, M. Jayasimhadri, T. Sasikala, L. Rama Moorthy, *Ceram. Int*., **39**, 8459–8465 (2013).
50. K. Linganna, Ch. Srinivasa Rao, C. K. Jayasankar. *J. Quant. Spectr. Radiat. Transfer*, **118**, 40–48 (2013).
51. K. Linganna, P. Haritha, K. Enkatta Krishnaiah, V. Venkatrmu, *Appl. Phys. B*, 1–12 (**2014**).
52. B. C. Jamalaiah, L. R. Moorthy, H. J. Seo, *J. Non-Cryst. Solids*, **358**, 204 (2012).
53. R. Reisfeld, E. Greenberg, R. Velapoldi, B. Barnett, *J. Chem. Phys*., **56**, 1698 (1972).